Journal of
Materials Chemistry A

Applying the HSAB Design Principle to the 3.5-V-class All-Solid-State Li-ion Batteries with a Chloride Electrolyte

SCHOLARONE™
Manuscripts

COMMUNICATION

Applying the HSAB Design Principle to the 3.5-V-class All-Solid-State Li-ion Batteries with a Chloride Electrolyte

Naoto Tanibata*, Shuta Takimoto, Shin Aizu, Hayami Takeda, Masanobu Nakayama

All-solid-state Li-ion batteries are expected to be the next generation of batteries with a high energy density and safety. However, for Li-ion batteries to endure high-voltage operations, the decomposition of solid electrolytes must be suppressed first. A high potential at the cathode tends to promote battery degradation because of the oxidation of the cathode electrolyte. This study aims to achieve the high-potential operation of all-solid-state batteries using $LiAlCl_4$ as a chloride electrolyte with a high oxidation resistance. However, batteries with commonly used oxide electrodes (*e.g.,* $LiFePO_4$) exhibit low capacity (~0.5 mAh g^{-1}), despite having working potentials less than the oxidation potential of $LiAlCl_4$. First-principles calculations and ^{27}Al MAS-NMR measurements suggest that acid–base reactions based on the hard and soft acid–base (HSAB) rule occur between the electrode and the electrolyte. In contrast, a high voltage of ~3.65 V (vs. Li^+/Li) and high-capacity utilisation (reversible capacity ~100 mAh g^{-1}) are observed at room temperature by combining the same chloride electrode (Li_2FeCl_4) without side reactions between these chlorides. These results indicate that material design based on the HSAB rule is also instructive when considering electrode/electrolyte material combinations, which realizes a 3.5-V-class all-solid-state Li-ion battery.

Introduction

Li-ion batteries (LIBs) have become indispensable in today's society mainly because they have higher operating voltages compared to other batteries.[1,2] However, this advantage requires the use of inflammable organic electrolytes that are stable under a high voltage. As a result, LIBs are not completely safe, and more work needs to be conducted to improve their safety.[3] This issue can be circumvented by using all-solid-state batteries with inorganic solid electrolytes as safer next-generation batteries.[4] Note that similar to liquid electrolytes, solid electrolytes are also required to display a high stability under high-voltage environments of LIBs.[5] The oxidation potential of the electrolyte is used as a design guideline for combining positive electrode/electrolyte materials.[6,7]

Although sulfide electrolytes are of research interest because many of them exhibit higher ionic conductivities than those of the oxide electrolytes,[8–10] their low oxidation resistances owing to the oxidation of sulfide ions, such as $S^{2-} \longrightarrow 1/2S_2^{2-} + e^-$, limit the available electric potential of positive electrodes (< ~2.5 V vs. Li^+/Li) and battery performance.[11–13] When combining sulfide electrolytes with cathode-active materials used in LIBs (such as $LiFePO_4$[14] and $LiCoO_2$[15]), the active material must have an oxide coating to prevent electrolyte oxidation and battery degradation.[16,17] However, coating treatments complicate the battery system and limit the choice of materials, in addition to being costly. Chloride electrolytes have recently been shown to possess higher oxidation resistances (oxidation window < ~4.6 V) than those of sulfide electrolytes because of the high electronegativity and high ionic conductivities.[18,19] For example, an all-solid-state battery using chloride electrolytes such as $Li_2In_xSc_{0.666-x}Cl_4$ showed high cycle performance (>3,000 cycles) without any coating of high-voltage cathode materials.[20] However, very few reports on batteries using chloride materials are available. Therefore, more studies should be carried out to draft design guidelines for using chloride battery materials. In a previous study, we explored potential solid chloride electrolytes with a high ionic conductivity through the exhaustive computational screening[21,22] of compounds in a structure database.[23] Our results showed that $LiAlCl_4$ had the most promising properties, such as migration energies for Li-ion conduction and phase stabilities (decomposition energies). In the present study, we aim to further the development of a solid-state electrode/electrolyte system with $LiAlCl_4$ to obtain guidelines for using chloride battery materials. Our experiments showed that the hard and soft acid–base (HSAB) rule,[24–26] which is a design guideline for acid–base reactions, is also important for selecting favourable electrode/electrolyte materials. As described below, Al^{3+} ions in $LiAlCl_4$ chloride electrolytes are classified as hard acids, and the use of electrodes with soft bases, which suppress side reactions, enables the high-voltage operation of all-solid-state Li batteries.

a. Department of Advanced Ceramics, Nagoya Institute of Technology, Gokiso, Showa, Nagoya, Aichi 466-8555, Japan
Corresponding author's e-mail: tanibata.naoto@nitech.ac.jp

Results and Discussion

Figure 1 shows the results of applying the LiAlCl$_4$ electrolyte to the commonly used LiFePO$_4$ positive electrode oxide. The charge–discharge curve (a) of the battery shows poor reversible capacity (<0.5 mAh g^{-1}). Similarly, LiCoO$_2$, another commonly used electrode material, also exhibits low capacity (Figure S1 (a)). As mentioned earlier, a high oxidation resistance of ~4.4 V vs Li$^+$/Li is suggested for LiAlCl$_4$ electrolytes, according to density functional theory (DFT) and convex hull-derived evaluations.[18] This value covers the charge/discharge working potentials of these cells; the upper cut-off potential is <4.4 V vs Li$^+$/Li. In other words, calculations that consider reactions involving only Li, Al, and Cl indicate that LiAlCl$_4$ is stable even at high-potential states in the cathode.

(a)

(b)
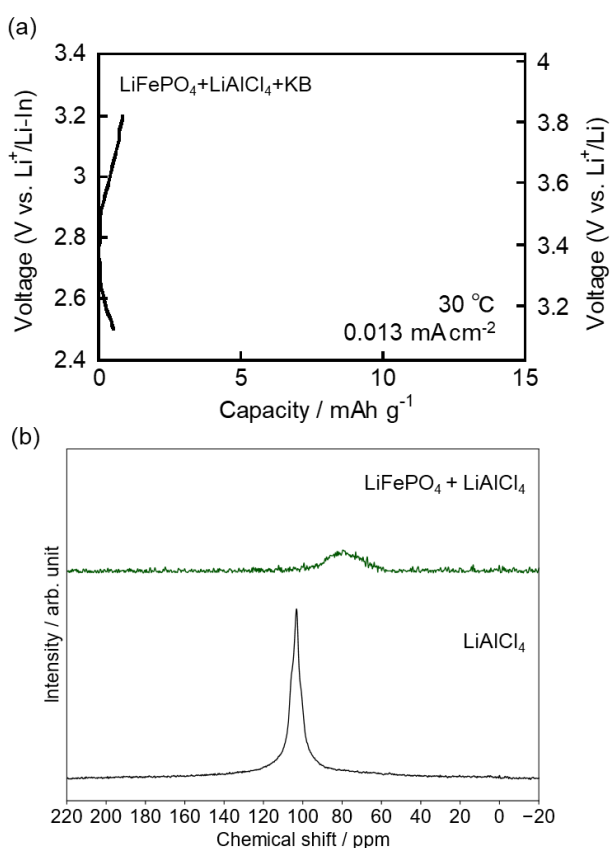
Figure 1. Evaluation of LiAlCl$_4$ and LiFePO$_4$ mixed material. (a) Charge–discharge curve of an all-solid-state Li-ion battery (LIB) with the mixed electrode composed of the LiFePO$_4$ electrode, LiAlCl$_4$ electrolyte, and conductive additive Ketjen black (KB). (b) ^{27}Al MAS-NMR spectra of LiAlCl$_4$ and the mixture of electrode active materials (LiFePO$_4$ + LiAlCl$_4$).

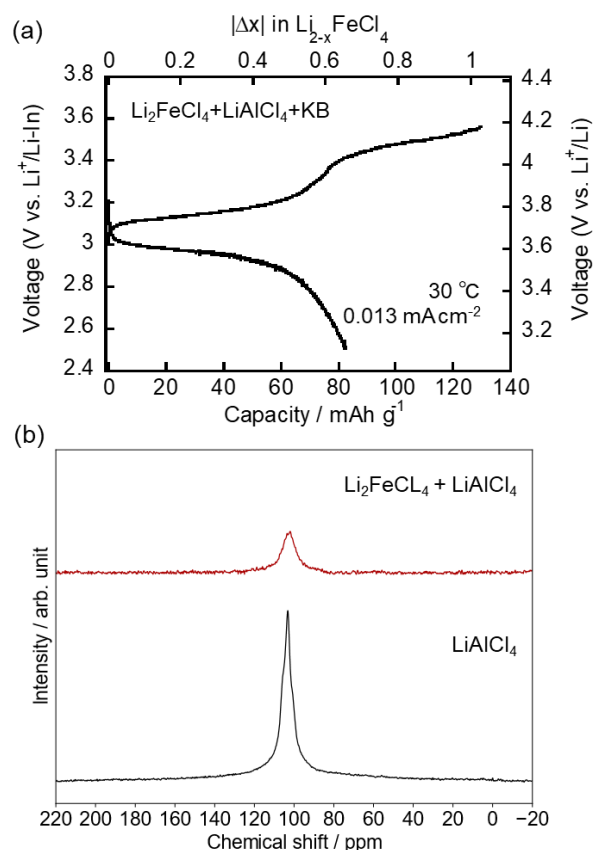Table 1. Reaction equations and corresponding decomposition energies for LiAlCl$_4$ and LiFePO$_4$ calculated using Interface Reaction App implemented in The Materials Project.[6,27]

In this respect, the energy diagram between the LiAlCl$_4$ electrolyte and the LiFePO$_4$ positive electrode was calculated using the Interface Reaction App implemented in The Materials Project.[6,27] The calculation suggested the existence of a negative formation energy between LiAlCl$_4$ and even uncharged LiFePO$_4$. Thus, contacting two compounds spontaneously causes a decomposition reaction, as shown in Table 1. In these reaction equations, the Al component of LiAlCl$_4$ is transformed into oxides, such as Al$_2$O$_3$ and AlPO$_4$, indicating an acid–base

reaction that changes the anion/cation combination. Such side reactions were confirmed by the ^{27}Al MAS-NMR spectra of the LiFePO$_4$ + LiAlCl$_4$ system shown in Figure 1(b). The tetrahedron-

Molar Fraction	Reaction Equation (normalized to reflect molar fraction)	Decomposition Energy [eV/atom]
0.000	LiAlCl$_4$ → LiAlCl$_4$	0.000
0.465	0.465 LiFePO$_4$ + 0.535 LiAlCl$_4$ → 0.38 LiFeCl$_4$ + 0.056 Al$_2$O$_3$ + 0.423 AlPO$_4$ + 0.042 Fe$_2$P + 0.62 LiCl	-0.059
0.500	0.5 LiFePO$_4$ + 0.5 LiAlCl$_4$ → 0.333 LiFeCl$_4$ + 0.5 AlPO$_4$ + 0.667 LiCl + 0.167 Fe	-0.062
0.667	0.667 LiFePO$_4$ + 0.333 LiAlCl$_4$ → 0.333 Fe$_2$PClO$_4$ + 0.333 AlPO$_4$ + LiCl	-0.071
1.000	LiFePO$_4$ → LiFePO$_4$	-0.000

derived peak observed for LiAlCl$_4$ at 103 ppm shifted to approximately 78 ppm and broadened in the mixture of LiAlCl$_4$ and LiFePO$_4$. The peak at a higher magnetic field was derived from the Al–O unit of aluminium oxides,[28,29] suggesting that LiAlCl$_4$ undergoes an acid–base reaction. Such side reactions have been suggested to occur at the chloride and oxide interface, resulting in rather low charge–discharge capacities. Therefore, the HSAB rule,[24–26] which is an empirical rule for acid–base reactions, was applied to find a reasonable combination of electrode–LiAlCl$_4$ electrolyte materials. LiAlCl$_4$ combines Al^{3+}, a hard acid with a small ionic radius, and Cl$^-$ ions, a borderline base. The O^{2-} ions in the oxides are hard bases with a higher charge density than those of Cl$^-$ ions.

(a)

(b)

Figure 2. Evaluation of LiAlCl$_4$–Li$_2$FeCl$_4$ mixed material. (a) Charge–discharge curve of all-solid-state LIB with the mixed electrode of Li$_2$FeCl$_4$ electrode, LiAlCl$_4$ electrolyte, and conductive additive KB (Ketjen black). (b) ^{27}Al MAS-NMR spectra of LiAlCl$_4$ and the mixture of electrode active materials (Li$_2$FeCl$_4$ + LiAlCl$_4$).

Table 2. Reaction equations and corresponding decomposition energies for $LiAlCl_4$ and Li_2FeCl_4 calculated using Interface Reaction App implemented in The Materials Project.[6,27]

Molar Fraction	Reaction Equation (normalized to reflect molar fraction)	Decomposition Energy [eV/atom]
0.000	$Li_2FeCl_4 \rightarrow 0.667\ LiFeCl_4 + 1.333\ LiCl + 0.333\ Fe$	-0.032
1.000	$LiAlCl_4 \rightarrow LiAlCl_4$	-0.000

Therefore, an acid–base reaction can be predicted to occur in $LiAlCl_4$ electrolytes upon contact with transition-metal-oxide electrodes. In addition, the calculated energies of decomposition of the other chloride materials exhibiting high ionic conductivities (Li_2ZrCl_6,[30] Li_3ScCl_6,[20] and Li_3InCl_6[31]) with $LiFePO_4$ are listed in Tables S1–S3. To analyse these data, the charge density index (Z/r^2) of the cations (Al^{3+}, Zr^{4+}, Sc^{3+}, In^{3+}) was plotted against the highest decomposition energy of each system (Fig. S3); here, Z is the formal charge of the cation, r is the ionic radius of the Shannon (6-coordination),[32] and Z/r^2 is a measure of the high charge density, or hardness of the cation. The energy of decomposition with $LiFePO_4$, which has the hard anion O^{2-}, increased with increasing hardness of the cation (Fig. S3). This suggests that the design guideline based on the acid–base reaction of the HSAB rule is also applicable to other material combinations. Using this design guideline, Li_2FeCl_4, which is also a chloride, was selected in this study as a high-voltage working material for combining with $LiAlCl_4$. As another idea, the use of oxide electrodes with cations harder than Fe^{2+} (such as Co^{3+} and Ni^{3+} in $LiCoO_2$ and $LiNiO_2$, respectively) could mitigate the effects of the side reactions derived from acid–base reactions with chloride electrolytes.

Li_2FeCl_4 has a high working potential (3.65 V vs Li^+/Li) because of the high electronegativity of chlorine, similar to the induced effect of the PO_4 unit in $LiFePO_4$ with the same Fe^{2+} ion.[33,34] The above acid–base reactions are expected to be suppressed if the electrode/electrolyte materials are both chlorides. In fact, the ^{27}Al MAS-NMR spectrum (Figure 2 (b)) shows a peak at the same position as the Al–Cl unit of $LiAlCl_4$ even after mixing, indicating that the degradation of $LiAlCl_4$ is suppressed. Table 2 shows the energy diagram between $LiAlCl_4$ and Li_2FeCl_4 calculated using the Interface Reaction App implemented in The Materials Project,[6,27] which indicates that no reaction between them exists in the database (only the thermodynamic decomposition of Li_2FeCl_4 at 0 K is shown). As depicted in Figure 2(a), the all-solid-state LIB using this composite operates at room temperature and shows a reversible capacity (82.5 mAh g^{-1}) that is more than 10 times higher than that of an oxide electrode. As shown above, an advanced battery was fabricated using a design guideline based on the acid–base reactivity in the electrolyte used as the cathode material, in addition to the generally accepted viewpoint of the oxidation potential (redox reaction). The second-voltage stage (~4.1 V vs Li^+/Li) of the charging curve (Fig. 3) appears to be irreversible; this probably originates from the Cl_2 desorption from the Li_2FeCl_4 chloride-type electrode during charging. Therefore, a cut-off was set at the first-stage termination voltage (3.82 V vs Li^+/Li), and a constant current–
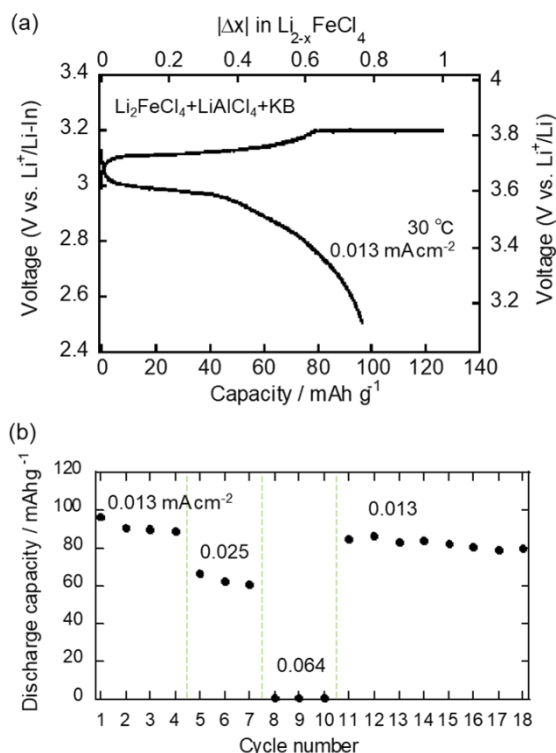
Figure 3. Charge–discharge performance of an all-solid-state LIB with $LiAlCl_4$ electrolyte applied to Li_2FeCl_4 electrode. (a) Constant current–constant voltage (CC–CV) charge–discharge curve at the first cycle. (b) Following cycle–rate characteristics at various constant current on the cut-off voltage of 3.82 V vs Li^+/Li.

constant voltage (CC–CV) was applied up to a capacity equivalent to one Li per Li_2FeCl_4 (126 mAh g^{-1}) during the first charge process. As a result, the reversibility and capacity improved to approximately 100 mAh g^{-1} (Figure 3(a)). Figure 3(b) shows the following cycle–rate characteristics at several constant current densities. Almost no capacity is observed at a current density of 0.064 mA cm^{-2} because the ionic conductivity of $LiAlCl_4$ is low at room temperature (~10^{-5} S cm^{-1}). However, the capacity at the 18th cycle, where the current density is the same as that at the 1st cycle, is almost the same as that of the initial cycle. This result is obtained owing to the suppression of side reactions, such as acid–base reactions, between the electrode and electrolyte. This result is the first step toward the realisation of all-solid-state batteries with a chloride electrode and chloride electrolyte; further improvements in the battery characteristics can be achieved by, for instance, optimising the composite ratio and shape of the conductive additive.

Conclusions

A chloride-type solid electrolyte with high oxidation resistance, $LiAlCl_4$, was applied to the 3.5-V-class all-solid-state LIB. Conventional oxide electrodes, such as $LiFePO_4$, showed a low charge/discharge capacity of ~0.5 mA h g^{-1}, whereas the use of Li_2FeCl_4 as the chloride electrode yielded a higher capacity of ~100 mA h g^{-1} at an operating voltage of ~3.6 V vs Li^+/Li and good capacity retention with cycling. The ^{27}Al NMR study and

thermodynamic calculations using the DFT-derived database confirmed the occurrence of decomposition due to the acid–base reaction at the interface of the oxide electrolyte and $LiAlCl_4$. The HSAB rule was established as a suitable guideline for finding a reasonable combination of electrode and electrolyte materials based on acid–base reactions. Although thermodynamic considerations using the DFT database can exhaustively consider the decomposition reaction scenario, they cannot consider unregistered compounds. However, only a limited number of chloride materials have been registered to date. In contrast, the application of the HSAB rule is more straightforward and useful for the intuitive screening of all battery materials, not just chlorides. Consequently, the combination of a chloride electrode and electrolyte is advantageous because of the oxidation potential limit and acid–base reactivity between the electrode and electrolyte, which permit the realisation of a 3.5-V-class all-solid-state Li^+ batteries only by compressing the powders.

Experimental Section

Fabrication of all-solid-state LIBs with $LiAlCl_4$ electrolyte

A schematic diagram of the all-solid-state battery used in the evaluation is shown in Figure S2. Cathode composites were obtained by mixing $LiAlCl_4$ with certain active materials (AMs; commonly used positive electrode oxides such as $LiFePO_4$ [Wako Pure Chemicals, 99.9%], $LiCoO_2$ [Sigma-Aldrich, 99.8%], and Li_2FeCl_4), and a conductive additive (Ketjenblack [KB], Lion Co.) at an $AM:LiAlCl_4:KB$ weight ratio of 7:2:1. Next, the $LiAlCl_4$ electrolyte was pressed at 96 MPa and ~5 mg of the prepared cathode composite was placed on top of the electrolyte pellet and pressed at 382 MPa. Finally, an all-solid-state LIB was fabricated by stacking a Li-In alloy as the anode (counter electrode).[35] Au-coated stainless steel with a diameter of 10 mm was used as the current collector. All the above operations, including the charging and discharging of the battery (by the VSP electrochemical analyser, BioLogic Co.), were carried out in a glove box under an argon gas atmosphere at 30 °C. The evaluation began with charging at a constant current density of 0.013 mA cm^{-2}.

NMR measurements of cathode composites

To investigate the chemical reactions in the cathode composites, ^{27}Al MAS-NMR measurements were performed on a mixture of $LiAlCl_4$ and cathode-active materials after heat treatment for 24 h at a temperature (130 °C) below the melting point of $LiAlCl_4$. The MAS spinning speed was 20 kHz in a Φ3.2-mm ZrO_2 rotor using a spectrometer (JNM-ECA600 II, JEOL RESONANCE Co., Ltd.). The 90° pulse width and relaxation delay were 2 μs and 5 s, respectively. The entire procedure was conducted under a dry Ar-filled atmosphere.

Quantum chemical reactivity investigation of electrode materials with $LiAlCl_4$ chloride electrolyte

The energy diagrams between the $LiAlCl_4$ electrolyte and $LiFePO_4$ or Li_2FeCl_4 positive electrode were calculated using the Interface Reaction App implemented in The Materials Project[6,27] to investigate the chemical reactions in the cathode composites.

Author Contributions

N. T. and M. N. conceived and designed the experiments: S. T. and S. A. performed the experiments and analysed the data: H. T. contributed materials/analysis tools: N. T. and M. N. co-wrote the paper.

Conflicts of Interest

There are no conflicts of interest to declare.

Acknowledgements

Notes and References

1   Z. Yang, J. Zhang, M. C. W. Kintner-Meyer, X. Lu, D. Choi, J. P. Lemmon and J. Liu, *Chem. Rev.*, 2011, **111**, 3577–3613.

2   S. Zhao, B. Wang, Z. Zhang, X. Zhang, S. He and H. Yu, *Electrochem. Energy Rev.*, 2022, **5**, 1–31.

3   J.-M. Tarascon and M. Armand, *Nature*, 2001, **414**, 359–367.

4   A. Manthiram, X. Yu and S. Wang, *Nat. Rev. Mater.*, 2017, **2**, 1–16.

5   J. Lau, R. H. DeBlock, D. M. Butts, D. S. Ashby, C. S. Choi, B. S. Dunn, J. Lau, R. H. DeBlock, D. M. Butts, D. S. Ashby, C. S. Choi and B. S. Dunn, *Adv. Energy Mater.*, 2018, **8**, 1800933.

6   W. D. Richards, L. J. Miara, Y. Wang, J. C. Kim and G. Ceder, *Chem. Mater.*, 2016, **28**, 266–273.

7   Y. Zhu, X. He and Y. Mo, *ACS Appl. Mater. Interfaces*, 2015, **7**, 23685–23693.

8   F. Mizuno, A. Hayashi, K. Tadanaga and M. Tatsumisago, *Adv. Mater.*, 2005, **17**, 918–921.

9   N. Kamaya, K. Homma, Y. Yamakawa, M. Hirayama, R. Kanno, M. Yonemura, T. Kamiyama, Y. Kato, S. Hama, K. Kawamoto and A. Mitsui, *Nat. Mater.*, 2011, **10**, 682–686.

10   J. Wu, L. Shen, Z. Zhang, G. Liu, Z. Wang, D. Zhou, H. Wan, X. Xu and X. Yao, *Electrochem. Energy Rev.*, 2021, **4**, 101–135.

11   T. Hakari, M. Deguchi, K. Mitsuhara, T. Ohta, K. Saito, Y. Orikasa, Y. Uchimoto, Y. Kowada, A. Hayashi and M. Tatsumisago, *Chem. Mater.*, 2017, **29**, 4768–4774.

12   F. Han, Y. Zhu, X. He, Y. Mo and C. Wang, *Adv. Energy Mater.*, 2016, **6**, 1501590.

13   J. Wu, S. Liu, F. Han, X. Yao, C. Wang, J. Wu, X. Yao, S. Liu, F. Han and C. Wang, *Adv. Mater.*, 2021, **33**, 2000751.

14   A. K. Padhi, K. S. Nanjundaswamy and J. B. Goodenough, *J. Electrochem. Soc.*, 1997, **144**, 1188–1194.

15   K. Mizushima, P. C. Jones, P. J. Wiseman and J. B. Goodenough, *Mater. Res. Bull.*, 1980, **15**, 783–789.

16   N. Ohta, K. Takada, L. Zhang, R. Ma, M. Osada and T. Sasaki, *Adv. Mater.*, 2006, **18**, 2226–2229.

17   N. Ohta, K. Takada, I. Sakaguchi, L. Zhang, R. Ma, K. Fukuda, M. Osada and T. Sasaki, *Electrochem. commun.*, 2007, **9**, 1486–1490.

18   X. Li, J. Liang, X. Yang, K. R. Adair, C. Wang, F. Zhao and X. Sun, *Energy Environ. Sci.*, 2020, **13**, 1429–1461.

19   S. Deng, M. Jiang, A. Rao, X. Lin, K. Doyle-Davis, J. Liang, C. Yu, R. Li, S. Zhao, L. Zhang, H. Huang, J. Wang, C. V. V. C. V. V. Singh, X. Sun, S. Deng, X. Lin, K. Doyle-Davis, J. Liang, C. Yu, R. Li, X. Sun, M. Jiang, A. Rao, C. V. V. C. V. V. Singh, S. Zhao, L. Zhang, J. Wang and H. Huang, *Adv. Funct. Mater.*, 2022, **32**, 2200767.

20   L. Zhou, T. T. T. Zuo, C. Y. Y. Kwok, S. Y. Y. Kim, A. Assoud, Q. Zhang, J. Janek and L. F. F. Nazar, *Nat. Energy*, 2022, **7**, 83–93.

21   M. Nakayama, K. Kanamori, K. Nakano, R. Jalem, I. Takeuchi and H. Yamasaki, *Chem. Rec.*, 2019, **19**, 771–778.

22   N. Tanibata, Y. Kondo, S. Yamada, M. Maeda, H. Takeda, M. Nakayama, T. Asaka, A. Kitajou and S. Okada, *Sci. Rep.*, 2018, **8**, 17199.

23   N. Tanibata, S. Takimoto, K. Nakano, H. Takeda, M. Nakayama and H. Sumi, *ACS Mater. Lett.*, 2020, **2**, 880–886.

24   T. L. Ho, *Chem. Rev.*, 2002, **75**, 1–20.

25   R. G. Pearson, *J. Chem. Educ.*, 1968, **45**, 581–587.

26   G. Sahu, Z. Lin, J. Li, Z. Liu, N. Dudney and C. Liang, *Energy Environ. Sci.*, 2014, **7**, 1053–1058.

27   A. Jain, S. P. Ong, G. Hautier, W. Chen, W. D. Richards, S. Dacek, S. Cholia, D. Gunter, D. Skinner, G. Ceder and K. A. Persson, *APL Mater.*, 2013, 1, 011002.

28   E. Witt, S. Nakhal, C. V. Chandran, M. Lerch and P. Heitjans, *Zeitschrift fur Phys. Chemie*, 2015, **229**, 1327–1339.

29   M. Licheron, V. Montouillout, F. Millot and D. R. Neuville, *J. Non. Cryst. Solids*, 2011, **357**, 2796–2801.

30   H. Kwak, D. Han, J. Lyoo, J. Park, S. Hoo Jung, Y. Han, G. Kwon, H. Kim, S. S.-T. Hong, K. K.-W. Nam, Y. Seok Jung, H. Kwak, J. Park, S. H. H. Jung, Y. Han, Y. S. S. Jung, H. Kim, D. Han, K. K.-W. Nam, J. Lyoo, S. S.-T. Hong and G. Kwon, *Adv. Energy Mater.*, 2021, **11**, 2003190.

31   X. Li, J. Liang, J. Luo, M. Norouzi Banis, C. Wang, W. Li, S. Deng, C. Yu, F. Zhao, Y. Hu, T. K. Sham, L. Zhang, S. Zhao, S. Lu, H. Huang, R. Li, K. R. Adair and X. Sun, 2019, **12**, 2665–2671.

32   R. D. Shannon, *Acta Crystallogr. Sect. A*, 1976, **32**, 751–767.

33   A. Kajiyama, K. Takada, T. Inada, M. Kouguchi, S. Kondo, M. Watanabe and M. Tabuchi, *Solid State Ionics*, 2002, **152–153**, 295–302.

34   N. Tanibata, M. Kato, S. Takimoto, H. Takeda, M. Nakayama and H. Sumi, *Adv. Energy Sustain. Res.*, 2020, **1**, 2000025.

35   K. Takada, N. Aotani, K. Iwamoto and S. Kondo, *Solid State Ionics*, 1996, **86–88**, 877–882.

36   K. Momma, F. Izumi and IUCr, *J. Appl. Crystallogr.*, 2008, **41**, 653–658.